

Syngas Conversion to C₂ Species over WC and M/WC (M = Cu or Rh) Catalysts: Identifying the Function of Surface Termination and Supported Metal Type

Wantong Zhao, Zun Guan, Debao Li, Baojun Wang,* Maohong Fan, and Riguang Zhang*



Cite This: *ACS Appl. Mater. Interfaces* 2022, 14, 19491–19504



Read Online

ACCESS |



Metrics & More



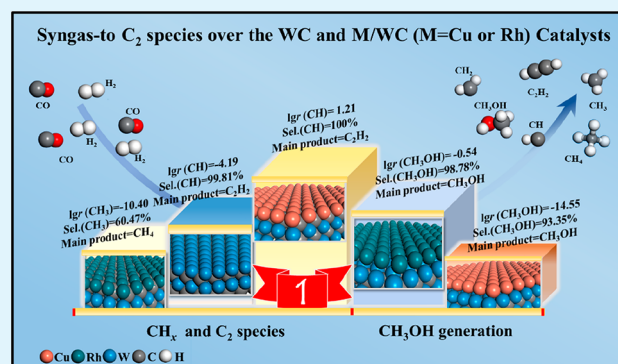
Article Recommendations



Supporting Information

ABSTRACT: Improving the selectivity and activity of C₂ species from syngas is still a challenge. In this work, catalysts with monolayer Cu or Rh supported over WC with different surface terminations (M/WC (M = Cu or Rh)) are rationally designed to facilitate C₂ species generation. The complete reaction network is analyzed by DFT calculations. Microkinetics modeling is utilized to consider the experimental reaction temperature, pressure, and the coverage of the species. The thermal stabilities of the M/WC (M = Cu or Rh) catalysts are confirmed by AIMD simulations. The results show that the surface termination and supported metal types in the M/WC (M = Cu or Rh) catalysts can alter the existence form of abundant CH_x (x = 1–3) monomer, as well as the activity and selectivity of CH_x monomer and C₂ species. Among these, only the Cu/WC–C catalyst is screened out to achieve outstanding activity and selectivity for C₂H₂ generation, attributing to that the synergistic effect of the subsurface C atoms and the surface monolayer Cu atoms presents the noble-metal-like character to promote the generation of CH_x and C₂ species. This work demonstrates a new possibility for rational construction of other catalysts with the non-noble metal supported by the metal carbide, adjusting the surface termination of metal carbide and the supported metal types can present the noble-metal-like character to tune catalytic performance of C₂ species from syngas.

KEYWORDS: syngas conversion, transition metals carbides, supported metal types, surface termination, CH_x intermediate



1. INTRODUCTION

Syngas (CO and H₂) conversion to C₂ species containing the oxygenates and hydrocarbons is a strongly exothermic, however, the low yield and selectivity become a challenge.^{1–3} Nowadays, although the widely used Rh-based catalyst has higher selectivity of C₂ oxygenate, it still has the shortcoming of high price and low CO conversion rate. Alternatively, the cheap Cu-based catalysts can present higher CO conversion rate;^{4,5} however, methanol formation is easier than CH_x formation, leading to low selectivity of C₂ species. Consequently, it is necessary to search for excellent catalyst that can promote the key intermediate CH_x formation from syngas and increase CO conversion rate.

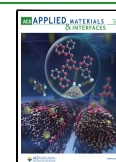
In recent years, the transition metal carbides act as catalytic materials to show unusually high activity, meanwhile, it is more stable under the reaction environment.⁶ More importantly, the transition metal carbides supported metal catalyst can well improve the catalytic performance of syngas conversion, for example, the Rh–Mn/W_xC catalyst enhanced the ability of CO conversion, as well as the productivity of higher alcohols from syngas.⁷ Cu/β-Mo₂C with W-termination promoted CO or CHO decomposition to produce CH, which is conducive to the generation of CHCHO via the reaction of CHO + CH →

CHCHO.⁸ Pt/WC exhibited an excellent CO poisoning resistance due to the existence of WC support.^{9–11} Furthermore, the different surface termination and supported metal types could alter the catalytic stability and catalytic performance of targeted reaction. For example, the termination of WC also impacts the stability of Rh₁₉/WC, Rh₃₁/WC and Rh₃₇/WC catalyst,¹² in which Rh₁₉ supported on WC with W-termination is the most stable compared with that on C-termination, while the Rh₃₁ and Rh₃₇ supported on C-termination is the most stable instead of W-termination. WC with C-termination more favors hydrogen production via NH₃ decomposition, while WC with W-termination is easily poisoned via N atoms, resulting in the difficult N atoms combinative desorption.¹³ WC with C-termination performs higher activity toward H₂O dehydrogenation to OH compared

Received: February 5, 2022

Accepted: April 13, 2022

Published: April 25, 2022



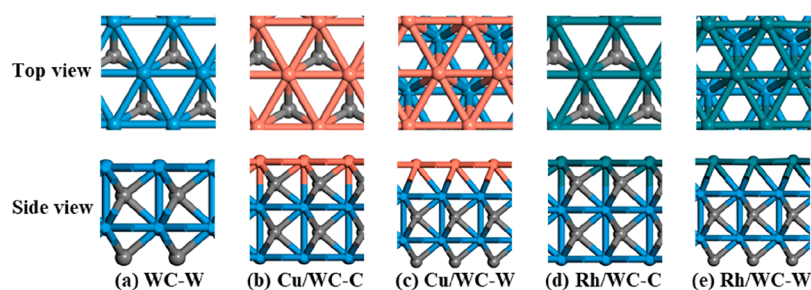


Figure 1. Top and side views for the optimized configurations of (a) WC–W, (b) Cu/WC–C, (c) Cu/WC–W, (d) Rh/WC–C, and (e) Rh/WC–W catalysts.

with that with W-termination.¹⁴ WC with W-termination easily activate CO into C and O atoms,¹⁵ and then the successive hydrogenation of C atom to generate CH_x ($x = 1-3$). Kovrega et al.¹⁶ studied CO_2 reduction over the Cu/WC–C and Cu/WC–W catalysts, in which the adsorption ability of CO and CO_2 over Cu/WC–C catalyst is weaker than that over Cu/WC–W catalyst, as a result, Cu/WC–C catalyst exhibits better catalytic performance toward CO_2 reduction. The Pt/WC–W and Pd/WC–C catalysts perform higher hydrogen oxidation/evolution reaction activity in comparison with the Pt/WC–C and Pd/WC–W catalysts, respectively.¹⁷ In summary, the different terminations of WC could greatly alter the catalytic performance and the stability of WC supported metal catalysts. However, up to now, few studies mentioned the influence of WC termination in the WC supported metal catalysts and the supported metal types on the catalytic performance of key CH_x intermediates and C_2 species generated from syngas, which remain unclear. Thus, it is significant to investigate the fundamental role of WC termination and the supported metal types in tuning the catalytic performance toward syngas converted to C_2 species over the WC supported Cu or Rh catalysts.

To clarify above issues, this work was carried out to systematically unravel the mechanism of syngas conversion to C_2 species over the WC supported the monolayer Cu or Rh catalysts, in which the C-termination and W-termination of WC are considered; meanwhile, the formation of abundant CH_x intermediate, the coupling of CH_x and CHO/CO reacting with CH_x to produce C_2 species are mainly examined. Moreover, the detailed analysis is carried out to identify the functions of WC termination and supported metal types, as well as the synergetic interaction between the Cu/Rh and WC in the M/WC ($M = \text{Cu}$ or Rh) catalysts. Here, DFT calculations, microkinetic modeling and ab initio molecular dynamics (AIMD) simulations are implemented. The densities of states and charge distribution are examined to reveal the determined factor to tune catalytic performance. It is hoped that the new possibility for rational construction of other catalysts with the non-noble metal supported by metal carbide are provided, in which adjusting the surface termination of metal carbide and the supported metal types can present the noble-metal-like character to tune the catalytic performance of C_2 species generation from syngas.

2. COMPUTATIONAL DETAILS

2.1. Calculation Methods. All spin-polarization calculations were implemented with the correlation functional of Perdew-Burke-Ernzerh (PBE) generalized gradient approximation (GGA).¹⁸ Vienna Ab-initio Simulation Package (VASP) was employed.¹⁹ A cutoff energy of 400 eV was adopted.

During structural optimization, the optimization convergence accuracy corresponds to $0.03 \text{ eV } \text{\AA}^{-1}$ and $1 \times 10^{-5} \text{ eV}$ toward the force and energy, respectively. A $(3 \times 3 \times 1)$ k -point mesh was employed to sample the Brillouin zone.²⁰ The transition states of all elementary steps are obtained via utilizing the climbing-image nudged elastic band method (CI-NEB).²¹ The dimer method²² was carried out based on the convergence less than $0.05 \text{ eV } \text{\AA}^{-1}$ to further optimize the transition state, which was further verified by the frequency analysis corresponding to the only one imaginary frequency.

2.2. Surface Models. WC catalyst is modeled by the most stable and mainly exposed (0001) surface, since the thermodynamically stability of WC(0001) with W termination is greater than that of WC(0001) with C termination,^{23,24} four-layer $p(3 \times 3)$ WC(0001) surface with W-termination is constructed, as shown in Figure 1a, which is denoted as WC–W. Aiming at improving the catalytic performance of Rh or Cu catalyst, the Rh or Cu monolayer is supported over the W-termination or C-termination of WC. As shown in Figure 1b–e, a $p(3 \times 3)$ Cu or Rh monolayer is supported over the three-layer $p(3 \times 3)$ WC with C-termination, denoted as Cu/WC–C and Rh/WC–C, respectively. Similarly, a $p(3 \times 3)$ Cu or Rh monolayer is supported over the three-layer $p(3 \times 3)$ WC with W-termination, denoted as Cu/WC–W and Rh/WC–W, respectively. During all calculations, the bottom two layers were fixed, and the other layers and substrates are relaxed. The interaction between the slabs is avoided by setting a 15 \AA vacuum.

3. RESULTS AND DISCUSSION

3.1. Catalysts Stability. The thermal stabilities of WC–W and M/WC ($M = \text{Cu}$ or Rh) catalysts are estimated using the AIMD simulation. Since C_2 species generation from syngas usually occurs at 500–623 K,^{2,25} the WC–W and M/WC ($M = \text{Cu}$ or Rh) catalysts are treated via performing the NVT ($T = 500 \text{ K}$) ensemble for 8 ps to achieve the equilibrium states. The NVT AIMD simulations are carried out using a Nose–Hoover thermostat.²⁶ The initial geometry of WC–W and M/WC ($M = \text{Cu}$ or Rh) catalysts was fully optimized, and then, AIMD simulations were carried out at 500 K for 8 ps with time step of 1 fs.^{27,28} This duration is also widely adopted to examine the thermal stability of other catalysts during AIMD simulations, for example, Saeed et al.²⁷ carried out AIMD simulations to analyze the thermal stability of monolayer MoC at 500, 1000, and 1500 K for 5 ps, suggesting that MoC can maintain its structural stability at 1000 K. AIMD simulations was carried out to analyze the thermal stability of Fe_2C_{12} , in which Fe_2C_{12} is very stable at 300 K without the significant migration for 6 and 12 ps.²⁸ As presented in Figure 2, the energy of WC–W and M/WC ($M = \text{Cu}$ or Rh) catalysts tend

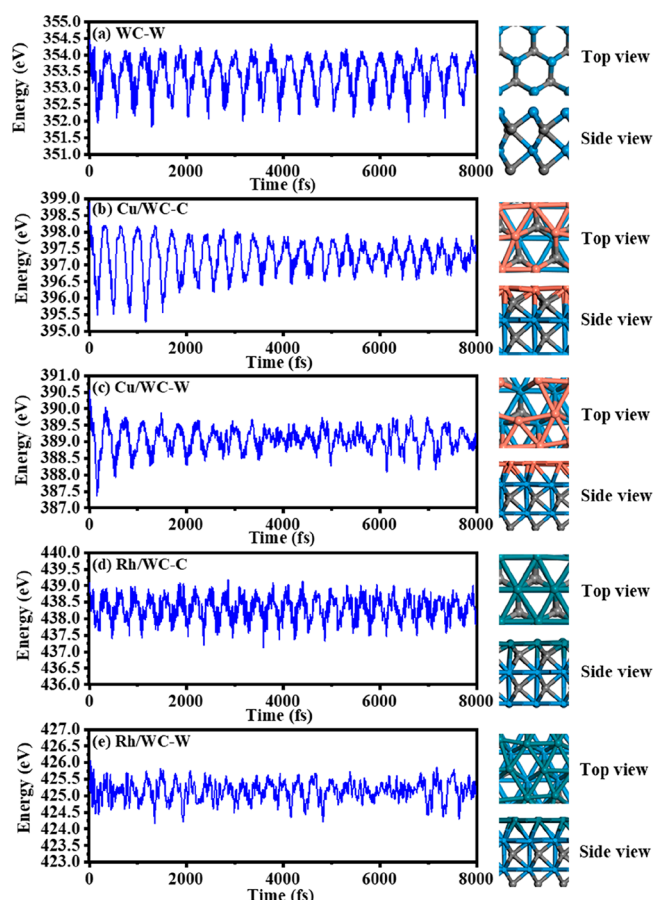


Figure 2. Energies against time during AIMD simulations for the (a) WC-W, (b) Cu/WC-C, (c) Cu/WC-W, (d) Rh/WC-C, and (e) Rh/WC-W catalysts; the top and side views of catalyst structure in the last snapshot are presented.

to be stable, suggesting that the M/WC (M = Cu or Rh) and WC-W catalysts have great thermal stability under the experimental condition of syngas conversion. Specifically, the deformation of Rh surface hardly occurs in Rh/WC-C; namely, Rh/WC-C has outstanding thermodynamic stability. However, the deformation of Rh or Cu surface occurs slightly in the Rh/WC-W, Cu/WC-C, and Cu/WC-W catalysts, respectively, confirming that the thermal stability of the M/WC (M = Cu or Rh) catalysts depends on the surface termination and supported metal types.

However, the binding energy (BE) between the metal atoms and the support can be used to evaluate the thermal stability of catalyst.^{11,29,30} For example, previous studies¹¹ showed that the binding energy between the Pt monolayer and WC greatly impacts the stabilization of the Pt monolayer over the WC surface, the stronger BE between the Pt atoms and WC with W-termination shows greater thermal stability than the WC with C-termination. Chen et al.³⁰ calculated the binding energy to reflect the thermal stability of M-C₃N₄ (M = Cu, Rh, Mn, Ag, Pt, Fe, Ni, Co, Pd, and Au), among them, Fe-C₃N₄ with the largest binding energy exhibits better thermal stability compared to other catalysts. Thus, to further analyze the thermal stability of M/WC (M = Cu or Rh) catalysts, the binding energy (BE) between WC and the supported metal atoms was calculated using eq 1:^{11,30}

$$BE = -(E_{\text{tot}} - E_{\text{WC}} - N \times E_M) / N \quad (1)$$

where E_{tot} , E_{WC} , and E_M represent the energies of M/WC (M = Cu and Rh), WC, and an isolated Cu or Rh atom, respectively. N is the atom number of supported metals.

The results show that the BE values of Cu/WC-C, Cu/WC-W, Rh/WC-C, and Rh/WC-W catalysts are 4.76, 3.82, 7.67, and 7.14 eV, respectively; that is, Rh/WC-C has

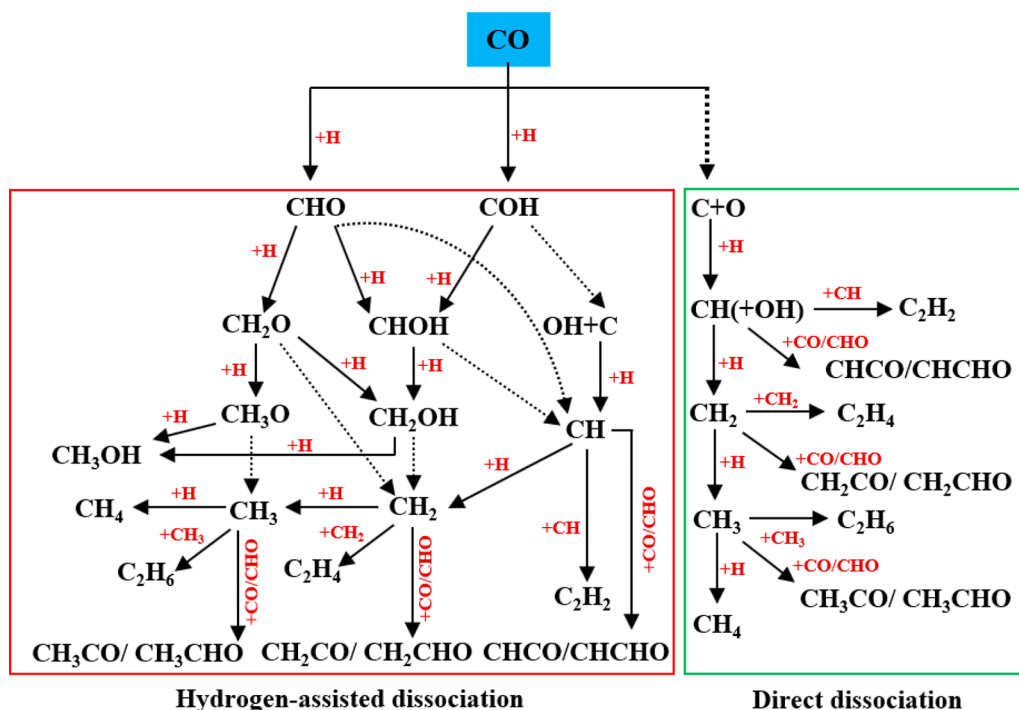


Figure 3. Possible reaction network of C₂ species generation from syngas over the WC-W, Cu/WC-C, Cu/WC-W, Rh/WC-C, and Rh/WC-W catalysts.

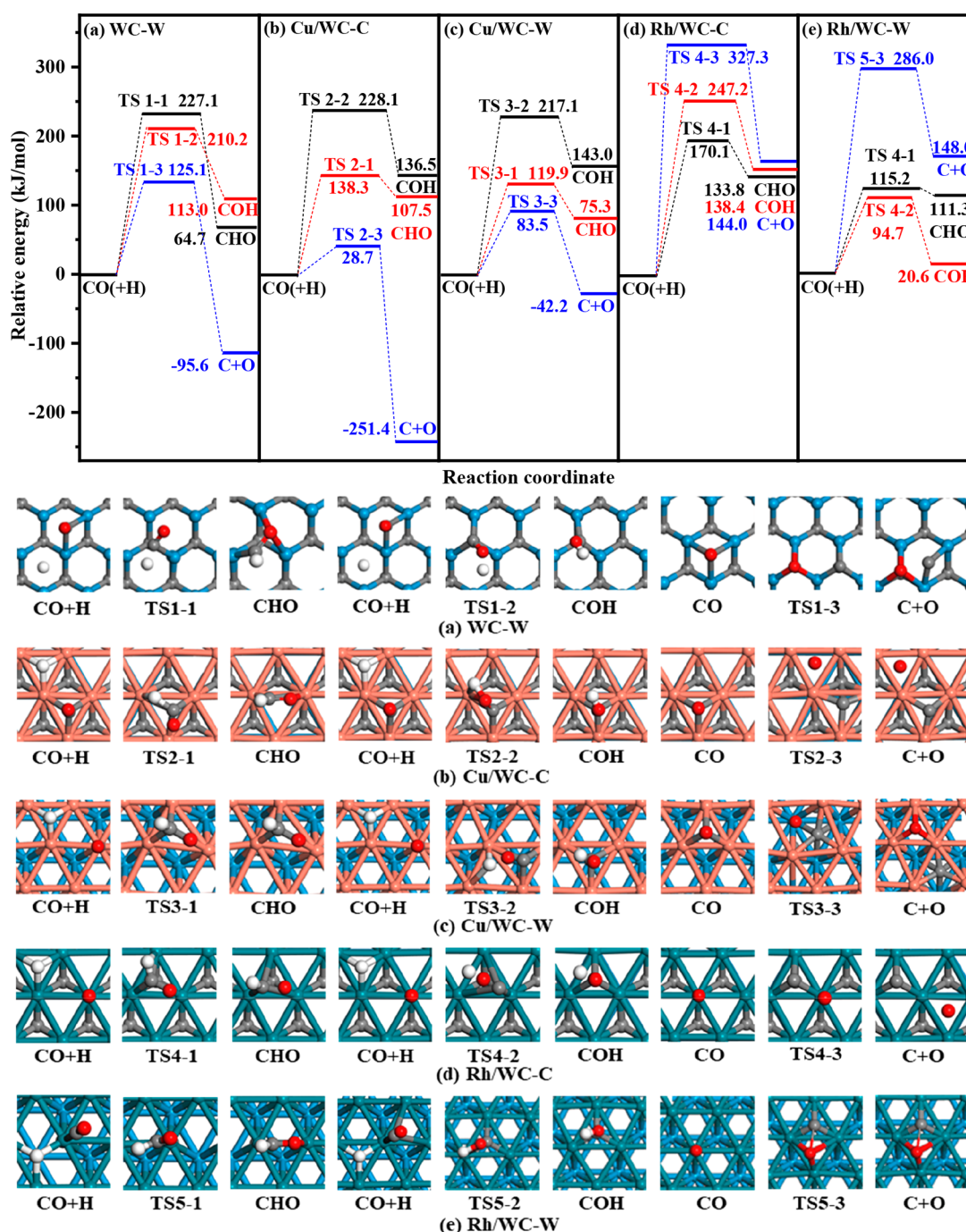


Figure 4. Free energy profile of CO direct dissociation and its hydrogenation over the (a) WC–W, (b) Cu/WC–C, (c) Cu/WC–W, (d) Rh/WC–C, and (e) Rh/WC–W catalysts together with the structures of initial states, transition states, and final states.

outstanding thermal stability corresponding to the strongest BE, which disfavors the deformation of Rh surface.

The previous experimental and theoretical studies showed that the M/WC catalysts show great stability, for example, Chhina et al.³¹ found that the WC catalyst has high thermal stability in the temperature range of 500–623 K, and it can serve as a catalyst support. The Cu/TiC³² and Cu/ δ -MoC³³ catalysts each exhibit great stability owing to the large binding energy between Cu atoms and TiC or δ -MoC in the process of CO₂ hydrogenation to CH₃OH at 550 K. Kelly et al.³⁴ found that Rh/WC catalyst has the outstanding stability during the decomposition of methanol at room temperature. Won et al.⁷

also reported the strong interaction between the Rh atoms and W_xC support results in Rh–Mn/W_xC catalyst with the great stability in syngas conversion to alcohol. Furthermore, based on above analysis, since syngas conversion to C₂ species often takes place at 500–623 K,^{2,25} it is concluded that the Cu or Rh monolayer supported on the WC catalysts could perform the great stability in syngas conversion to C₂ species. More importantly, the previously theoretical studies also showed that the binding energy between the monolayer Rh atoms and WC catalyst with C-termination in Rh/WC–C catalyst (~ 7.10 eV) is much stronger than that between the monolayer Cu atoms and the WC catalyst with C-termination in Cu/WC–C catalyst

(~ 4.10 eV).³⁵ Similarly, Sun et al.³⁶ also experimentally found that Rh/MoC_x catalyst shows a higher stability than that of the Cu/MoC_x catalyst, which could be attributed to the strong binding energy between Rh atoms and MoC_x catalyst to inhibit the oxidation of carbides induced by H₂O in water-gas-shift reaction at 574 K. These reported results indirectly and directly supported our calculated results that Rh/WC-C catalyst shows a higher stability due to the strong binding energy between Rh atoms and WC, and their thermal stability depend on the supported metal types.

3.2. Generation Path of C₂ Species and Byproduct from Syngas. As presented in Figure 3, two crucial steps exist:^{37,38} The first is CO conversion to produce the key intermediate CH_x; the other is the generation of C₂ oxygenates precursor CH_xCO ($x = 1-3$) via CO reacting with CH_x, as well as the coupling of CH_x to C₂ hydrocarbons. For the generation of the key CH_x intermediate, two possible paths exist: The C-O bond ruptured in CH_xO/CH_xOH formed by CO hydrogenation and the rupture of C-O bond in CO to produce C and O atoms; subsequently, the C atom is hydrogenated to generate CH_x ($x = 1-3$). Alternatively, CH_xO/CH_xOH can be continuously hydrogenated to CH₃OH, which decreases the selectivity of the key intermediate CH_x ($x = 1-3$). Meanwhile, the hydrogenation of CH_x ($x = 1-3$) to methane decreases the productivity of C₂ species. Table S2 lists the activation free energy and reaction free energy of all the mentioned reactions at 500 K for syngas conversion over the WC-W and M/WC (M = Cu or Rh) catalysts.

3.3. H₂ Adsorption and Dissociation, as Well as CO Initial Activation. **3.3.1. H₂ Adsorption and Dissociation.** Since H₂ dissociation is a key step to provide hydrogen source for CO hydrogenation, the adsorption and dissociation of H₂ was first investigated over the M/WC (M = Cu or Rh) and WC catalysts, as shown in Figures S2 and S3; H₂ dissociative adsorption occurs spontaneously to form adsorbed H atoms over the Cu/WC-C, Rh/WC-C, Rh/WC-W and WC catalysts. However, molecular adsorption H₂ occurs on Cu/WC-W catalyst, as presented in Figure S3, the dissociation of molecular adsorption H₂ on Cu/WC-W catalyst has very small activation free energies of 33.5 kJ·mol⁻¹ at 500 K. Thus, the dissociation of H₂ into H atom over the M/WC (M = Cu or Rh) and WC catalysts easily occurs, which can provide abundant hydrogen source to participate into the hydrogenation reaction. Namely, H₂ dissociation is not the rate-determined step in syngas-to-C₂ species, which does not affect the activity of syngas-to-C₂ species over the M/WC (M = Cu or Rh) and WC catalysts.

3.3.2. CO Initial Activation. CO initial activation plays a vital role in syngas conversion,³⁻⁵ which mainly included CO hydrogenation to CHO/COH and CO direct decomposition into C and O (Figure 4) CO kinetically prefers the direct decomposition (125.1, 28.7, and 83.5 kJ·mol⁻¹) rather than the hydrogenation of CO to generate CHO/COH over the WC-W, Cu/WC-C, and Cu/WC-W catalysts; CO direct decomposition is an exothermic process by 95.6, 251.4, and 42.2 kJ·mol⁻¹. Meanwhile, our previous studies³ showed that CO is easily hydrogenated to produce CHO (105.8 kJ·mol⁻¹) over Cu(111). Thus, WC support in the Cu/WC-C and Cu/WC-W catalysts could alter the optimal path of CO activation and effectively enhance the ability of CO activation compared to Cu catalyst (28.7 and 83.5 vs 105.8 kJ·mol⁻¹). Furthermore, the previous experiment found that CO direct decomposition

into C and O easily occurs over the WC-W and Mo₂C catalysts, which indirectly and directly support our results. For example, Kelly et al.³⁴ theoretically and experimentally found that WC catalyst is responsible for C-O bond breakage of CH₃OH to generate CH₄. Ren et al.³⁹ experimentally showed that the WC-W catalyst prefers the C-O bond cleavage during the process of C₃ oxygenates conversion to propene. Kelly et al.⁴⁰ found that the bare Mo₂C surface was active for the C-O breakage of ethanol to generate ethylene.

The Rh/WC-C catalyst kinetically prefers the reaction of CO + H → CHO (170.1 kJ·mol⁻¹) in comparison with CO → C + O and CO + H → COH. However, COH generation (94.7 kJ·mol⁻¹) over Rh/WC-W catalyst is preferable kinetically; our previous studies⁴¹ showed that Rh(111) prefers the reaction of CO + H → CHO (139.9 kJ·mol⁻¹) rather than the reactions of CO + H → COH and CO → C + O. Thus, compared to the Rh catalyst, the exposed termination of WC support in the Rh/WC catalysts can change the optimal CO activation path, especially the Rh/WC-W catalyst enhances the ability of CO initial activation.

The above analysis shows that the Cu/WC-C catalyst has a higher CO activation ability in comparison with the Cu/WC-W catalyst, so the C-termination is more preferable for CO activation in the Cu/WC catalysts. However, the W-termination is more preferable for CO activation in the Rh/WC catalysts. Among the five types of catalysts, the Cu/WC-C catalyst has the highest CO initial activation ability.

3.4. Optimal Path of CH_x ($x = 1-3$) and Methanol Formation. For the CH_x ($x = 1-3$) and CH₃OH generation, all possible reaction paths in Figure 3 are considered (see details in the Supporting Information); Figure 5 only presents the optimal path of CH_x ($x = 1-3$) and methanol formation over these five types of catalysts.

For CH generation, over the WC-W, Cu/WC-W, and Cu/WC-C catalysts (Figures 5a-c), the path of CO + H → C + O + H → CH + O is a dominant process. Meanwhile, previous results³ show that CH generation mainly originated from the process of CO + H → CHO + (H) → CHOH → CH + OH over Cu(111). Thus, compared to the Cu catalyst, the WC support in the Cu/WC-W and Cu/WC-C catalysts alters the optimal path of CH generation. In Figure 5d,e, over the Rh/WC-C and Rh/WC-W, the process of CO + H → COH + (H) → CHOH → CH + OH is kinetically favored; however, the process of CO + H → CHO + (H) → CHOH → CH + OH is kinetically favored over Rh(111);⁴¹ namely, WC support changes the optimal path of CH generation.

For CH₂ generation, as shown in Figure 5a,b, over the WC-W and Cu/WC-C catalysts, the process of CO + (H) → C + O + (H) → CH + (H) → CH₂ is more feasible. Over Cu/WC-W (see Figure 5c), CH₂ generation is mainly from CO + H → CHO + (H) → CH₂O + (H) → CH₂OH → CH₂+OH. Previous results over Cu(111)³ showed that the optimal process of CH₂ generation is CO + H → CHO + (H) → CHOH + H → CH₂OH → CH₂+OH. Thus, compared to Cu catalyst, the WC support in Cu/WC-C catalyst changes the optimal path of CH₂ generation. Over the Rh/WC-C and Rh/WC-W catalysts (see Figure 5d,e), the process of CO + H → COH + (H) → CHOH → CH + OH + (H) → CH₂ + OH is more kinetically favored; however, CH₂ generation mainly undergoes the process of CO + H → CHO + (H) → CH₂O → CH₂+O over Rh(111);⁴¹ namely, the optimal path of CH₂ generation depended on the WC support.

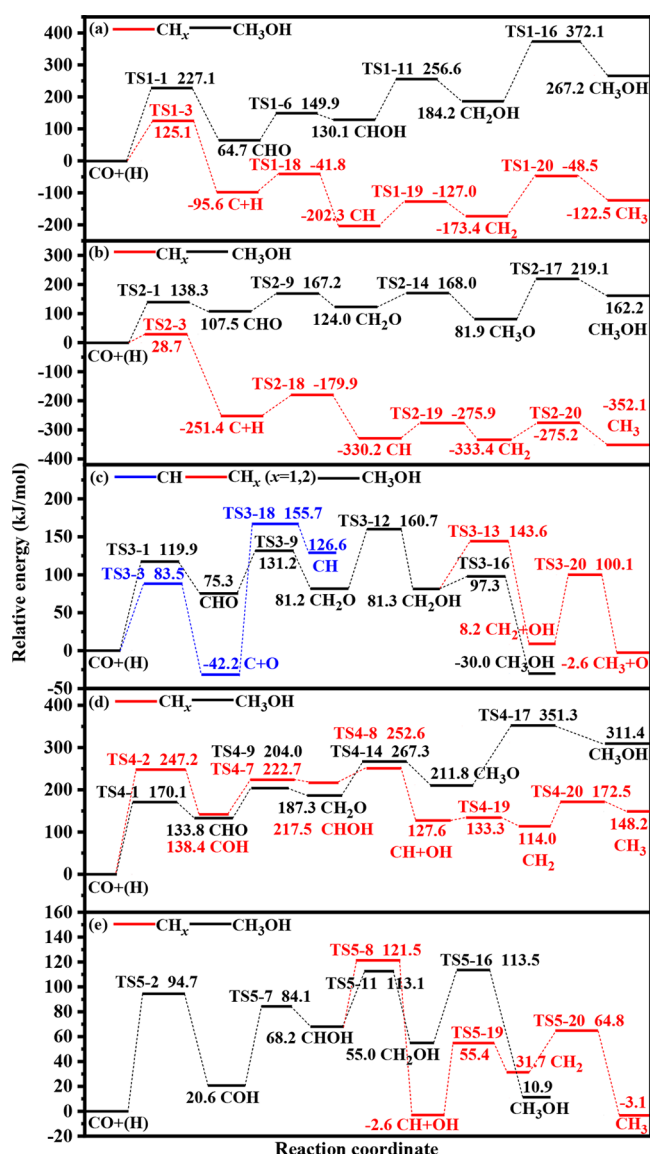


Figure 5. Potential energy profile for the optimal path of CH_x ($x = 1-3$) and CH_3OH production over the (a) WC-W, (b) Cu/WC-C, (c) Cu/WC-W, (d) Rh/WC-C, and (e) Rh/WC-W catalysts. The corresponding structure are presented in Figures S4–S9.

For CH_3 generation, as shown in Figure Sa,b, over the WC-W and Cu/WC-C catalysts, $\text{CO} + (\text{H}) \rightarrow \text{C} + \text{O} + (\text{H}) \rightarrow \text{CH} + (\text{H}) \rightarrow \text{CH}_2 + (\text{H}) \rightarrow \text{CH}_3$ is dominant. Over Cu/WC-W (see Figure 5c), CH_3 generation mainly undergoes the process of $\text{CO} + \text{H} \rightarrow \text{CHO} + (\text{H}) \rightarrow \text{CH}_2\text{O} + (\text{H}) \rightarrow \text{CH}_2\text{OH} \rightarrow \text{CH}_2 + \text{OH} + (\text{H}) \rightarrow \text{CH}_3 + \text{OH}$. However, previous results over Cu(111)³ showed that CH_3 generation mainly undergoes the process of $\text{CO} + \text{H} \rightarrow \text{CHO} + (\text{H}) \rightarrow \text{CH}_2\text{O} + (\text{H}) \rightarrow \text{CH}_3\text{O} \rightarrow \text{CH}_3 + \text{O}$. Thus, the WC support in the Cu/WC-C and Cu/WC-W catalysts changes the optimal path of CH_3 generation in comparison with Cu catalyst. Furthermore, as shown in Figure 5d,e, over the Rh/WC-C and Rh/WC-W catalysts, the process of $\text{CO} + \text{H} \rightarrow \text{COH} + (\text{H}) \rightarrow \text{CHOH} \rightarrow \text{CH} + \text{OH} + (\text{H}) \rightarrow \text{CH}_2 + (\text{H}) \rightarrow \text{CH}_3$ is more kinetically favored. Over Rh(111),⁴¹ CH_3 is mainly originated from the process of $\text{CO} + \text{H} \rightarrow \text{CHO} + (\text{H}) \rightarrow \text{CH}_2\text{O} + (\text{H}) \rightarrow \text{CH}_3\text{O} \rightarrow \text{CH}_3 + \text{O}$. Thus, the optimal path of CH_3 generation is greatly impacted by WC support.

The above analysis about the optimal path of CH_x generation indicates that the generation of CH is first, and then CH_2 and CH_3 are formed via CH hydrogenation; namely, CH can serve as the precursor to generate CH_2 and CH_3 .

For CH_3OH generation (Figure 5a), over WC-W, $\text{CO} + \text{H} \rightarrow \text{CHO} + (\text{H}) \rightarrow \text{CHOH} + (\text{H}) \rightarrow \text{CH}_2\text{OH} + (\text{H}) \rightarrow \text{CH}_3\text{OH}$ is dominant. Over Cu/WC-C (Figure 5b), CH_3OH is mainly from the process of $\text{CO} + \text{H} \rightarrow \text{CHO} + (\text{H}) \rightarrow \text{CH}_2\text{O} + (\text{H}) \rightarrow \text{CH}_3\text{O} + (\text{H}) \rightarrow \text{CH}_3\text{OH}$. Over Cu/WC-W (Figure 5c), $\text{CO} + \text{H} \rightarrow \text{CHO} + (\text{H}) \rightarrow \text{CH}_2\text{O} + (\text{H}) \rightarrow \text{CH}_2\text{OH} + (\text{H}) \rightarrow \text{CH}_3\text{OH}$ is more kinetically favored. Meanwhile, previous results³ show that CH_3OH generation over Cu(111) mainly undergoes the process of $\text{CO} + \text{H} \rightarrow \text{CHO} + (\text{H}) \rightarrow \text{CH}_2\text{O} + (\text{H}) \rightarrow \text{CH}_2\text{OH} + (\text{H}) \rightarrow \text{CH}_3\text{OH}$ and $\text{CO} + \text{H} \rightarrow \text{CHO} + (\text{H}) \rightarrow \text{CHOH} + (\text{H}) \rightarrow \text{CH}_2\text{OH} + (\text{H}) \rightarrow \text{CH}_3\text{OH}$. Thus, the WC support in Cu/WC-C changes the optimal path of CH_3OH generation compared to the Cu catalyst. Furthermore, (Figure 5d), over Rh/WC-C, the process of $\text{CO} + \text{H} \rightarrow \text{CHO} + (\text{H}) \rightarrow \text{CH}_2\text{O} + (\text{H}) \rightarrow \text{CH}_3\text{O} + (\text{H}) \rightarrow \text{CH}_3\text{OH}$ is more feasible. Over Rh/WC-W (Figure 5e), the process is $\text{CO} + \text{H} \rightarrow \text{COH} + (\text{H}) \rightarrow \text{CHOH} + (\text{H}) \rightarrow \text{CH}_2\text{OH} + (\text{H}) \rightarrow \text{CH}_3\text{OH}$. Over Rh(111),⁴¹ CH_3OH is generated mainly via the process of $\text{CO} + \text{H} \rightarrow \text{CHO} + (\text{H}) \rightarrow \text{CH}_2\text{O} + (\text{H}) \rightarrow \text{CH}_3\text{O} + (\text{H}) \rightarrow \text{CH}_3\text{OH}$. Thus, the optimal path of CH_3OH generation greatly depends on the WC support.

3.5. Abundant CH_x ($x = 1-3$) Monomer. As shown in Figure 6a, the generation of CH, CH_2 , and CH_3 through the optimal path have the same overall barriers over the WC-W (125.1 $\text{kJ}\cdot\text{mol}^{-1}$), Cu/WC-C (28.7 $\text{kJ}\cdot\text{mol}^{-1}$), Rh/WC-C (252.6 $\text{kJ}\cdot\text{mol}^{-1}$), and Rh/WC-W (121.5 $\text{kJ}\cdot\text{mol}^{-1}$) catalysts, so CH, CH_2 , and CH_3 could serve as the abundant CH_x monomer, in which CH is the precursor to generate CH_2 and CH_3 ; namely, CH is the abundant CH_x monomer. However, CH generation requires a lower overall barrier compared to CH_2 and CH_3 generation over Cu/WC-W catalyst (155.7 vs 160.7 and 160.7 $\text{kJ}\cdot\text{mol}^{-1}$), suggesting that CH should be the abundant CH_x monomer. Furthermore, previous studies showed that the abundant CH_x monomer were both CH_2 and CH_3 with the overall barriers of 149.3 and 145.6 $\text{kJ}\cdot\text{mol}^{-1}$ over the Cu(111) surface,³ whereas CH serves as the abundant CH_x monomer over Rh(111) surface, which requires the overall barrier of 225.9 $\text{kJ}\cdot\text{mol}^{-1}$.⁴¹

More importantly, compared to the Cu catalyst, the Cu/WC-C catalyst greatly enhances the activity of the abundant CH_x monomer (149.3 and 145.6 vs 28.7 $\text{kJ}\cdot\text{mol}^{-1}$), while the Cu/WC-W catalyst decreases the activity of the abundant CH_x monomer (155.7 vs 149.3 and 145.6 $\text{kJ}\cdot\text{mol}^{-1}$). Similarly, compared to the Rh catalyst, the Rh/WC-W catalyst increases the activity of the abundant CH_x monomer (121.5 vs 225.9 $\text{kJ}\cdot\text{mol}^{-1}$), whereas the Rh/WC-C catalyst reduces the activity of the abundant CH_x monomer (252.6 vs 225.9 $\text{kJ}\cdot\text{mol}^{-1}$).

Thus, the WC support in the M/WC ($M = \text{Cu}$ or Rh) catalysts alters the existence form of the abundant CH_x monomer, and its generation activity compared to the Cu and Rh catalysts. Moreover, the exposed surface termination of WC can also change the activity of the abundant CH_x monomer.

4. GENERAL DISCUSSIONS

4.1. Influences of Surface Termination and Supported Metal Types on CO Activation. Above analysis results show that the reactivity of CO activation is closely

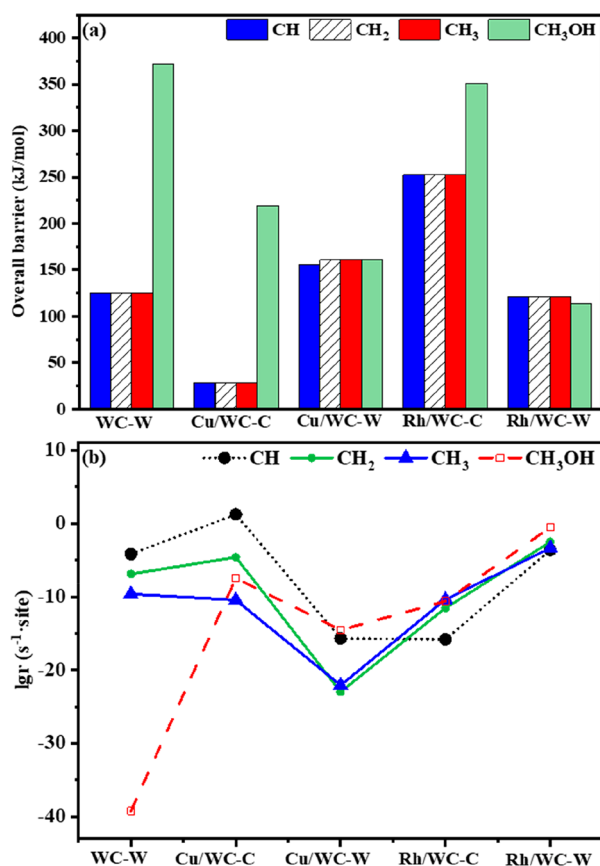


Figure 6. (a) Overall barrier ($\text{kJ}\cdot\text{mol}^{-1}$) at 500 K for the optimal path of CH_x ($x = 1-3$) and CH_3OH production based on the DFT calculations. (b) Rate ($\text{molecules}\cdot\text{s}^{-1}\cdot\text{site}^{-1}$) at 500 K of CH_x ($x = 1-3$) and CH_3OH production from syngas based on the microkinetic modeling over the WC-W, Cu/WC-C, Cu/WC-W, Rh/WC-C, and Rh/WC-W catalysts.

linked with the surface termination and supported metal types. First, on the basis of the geometric parameters, the WC-W, Cu/WC-C, and Cu/WC-W catalysts prefer direct CO decomposition into C and O atoms, whereas the Rh/WC-C and Rh/WC-W catalysts contribute to CHO or COH generation by CO hydrogenation, which is attributed to different C–O bond lengths in the activated CO. Specifically, the C–O bond lengths in CO over the WC-W (1.205 Å), Cu/WC-C (1.189 Å), and Cu/WC-W (1.186 Å) catalysts are longer than those over the Rh/WC-C (1.168 Å) and Rh/WC-W (1.164 Å) catalysts; correspondingly, the C–O bond rupture of CO more easily occurs over the WC-W, Cu/WC-C, and Cu/WC-W catalysts.

However, the change of CO activation ability could be attributed to the difference of CO adsorption energy caused by the change of electronic properties, such as *d*-band center of surface.⁴² The adsorption energies of CO at 500 K are -158.1 , -131.9 , -94.5 , -82.9 , and -69.5 $\text{kJ}\cdot\text{mol}^{-1}$ over the Rh/WC-C, WC-W, Cu/WC-C, Rh/WC-W and Cu/WC-W catalysts, respectively; correspondingly, the *d*-band center follows the sequence WC-W and Rh/WC-W (-2.20 eV) > Cu/WC-C (-2.54 eV) > Cu/WC-W (-2.60 eV) > Rh/WC-C (-2.83 eV). The moderate CO adsorption ability on Cu/WC-C catalyst corresponds to the moderate *d*-band center; as a result, the C–O bond cleavage of CO easily occurs to show high CO activation ability on Cu/WC-C catalyst.

However, CO adsorption ability is too weak or too strong over the WC, Cu/WC-W, Rh/WC-C, and Rh/WC-W catalysts with the *d*-band center either too far or too close from the Fermi level; thus, the C–O bond activation of CO becomes difficult, leading to the weaker CO activation ability. Furthermore, CO activation ability affects the activity of CH_x ($x = 1-3$) monomers generation.

4.2. Influences of Surface Termination and Supported Metal Types on the Activity of the Abundant CH_x ($x = 1-3$) Monomer Based on Microkinetic Modeling. The reaction pressure and the coverage of intermediate species also greatly affect the activity and selectivity of product; for example, DFT calculations by Braga et al.⁴³ showed that the activation barrier of the metallocarbene reacting with a diazo molecule (dimerization reaction) is lower than that of the metallocarbene reacting with alkane (alkane activation), which is not consistent with the experimental conclusion that the high activity corresponds to alkane activation, this situation is attributed to that the high coverage of alkane is not considered, resulting in the lower rate of dimerization compared with alkane activation. Moreover, the reaction pressure also affects the activity of ammonia synthesis on Fe catalyst, and the reaction rate increases with the pressure increasing.⁴⁴ Based on above analysis, the generation of the abundant CH_x ($x = 1-3$) monomer is significant for C_2 species. Aiming at elucidating the influences of the surface termination and supported metal types on the activity of the abundant CH_x ($x = 1-3$) monomer under the actually experimental condition, the generation rate of syngas conversion to CH_x is estimated by microkinetics modeling⁴⁵ over the WC-W and M/WC ($M = \text{Cu}$ or Rh) catalysts, which consider the impacts of the reaction temperature and pressure, the coverage of the species (see details in the Supporting Information).

As shown in Figure 6b, microkinetics modeling shows that over the WC-W, Cu/WC-C, and Cu/WC-W catalysts, CH serves as the abundant CH_x monomer. However, CH_2 and CH_3 serve as the abundant CH_x monomer over Cu(111).³ Over the Rh/WC-C and Rh/WC-W catalysts, CH_3 and CH_2 serve as the abundant CH_x monomer, respectively, whereas CH serves as the abundant CH_x monomer over Rh(111).⁴¹ The WC support in the M/WC-C ($M = \text{Cu}$ or Rh) catalysts impacts the existence of the abundant CH_x monomer in comparison with the Cu and Rh catalysts. Meanwhile, the generation rate ($\text{s}^{-1}\cdot\text{site}^{-1}$) of the abundant CH_x monomer follows the sequence Cu/WC-C (1.65×10^1) > Rh/WC-W (2.89×10^{-3}) > WC-W (6.32×10^{-5}) > Rh/WC-C (4.00×10^{-11}) > Cu/WC-W (2.04×10^{-16}); namely, Cu/WC-C presents the highest activity toward abundant CH_x monomer. Thus, the synergistic effect of the C-termination and the monolayer M in the M/WC-C ($M = \text{Cu}$ or Rh) catalyst presents excellent activity toward abundant CH_x monomer, which is also supported by the previously reported studies; for example, the AuPt/WC with W-termination is more preferable for H_2 dissociation compared to the Au(111) surface.⁴⁶ The Pt or PtRu monolayer supported over $\text{Ti}_{0.1}\text{W}_{0.9}\text{C}$ catalysts achieves higher activity toward methanol electrooxidation compared to the Pt catalyst.⁴⁷

Furthermore, as shown in Figure 7, the relationship between the *d*-band center of surface metal atoms and the rate of abundant CH_x monomer generation presents a volcano-shaped curve over the WC-W and M/WC ($M = \text{Cu}$ or Rh) catalysts, in which the moderate *d*-band center of Cu/WC-C

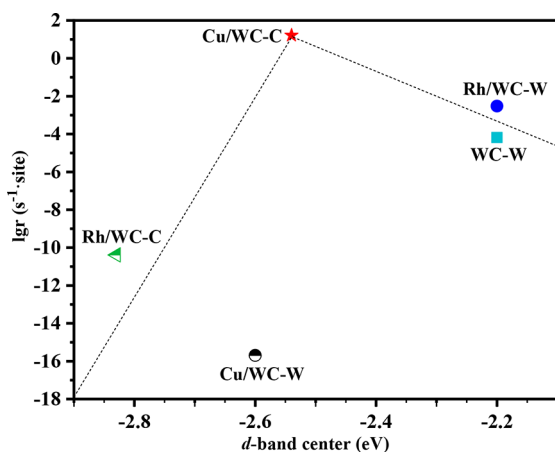


Figure 7. Relationship of d -band center of surface metal atoms with the activity of the abundant CH_x monomer over the WC-W, Cu/WC-C, Cu/WC-W, Rh/WC-C, and Rh/WC-W catalysts.

corresponds to the highest activity of abundant CH_x monomer. Moreover, previous reports also showed that the moderate d -band center carried out the best catalytic performance;^{48,49} for example, the activity of 2-propanol dehydrogenation over the M/SiO_2 ($\text{M} = \text{Ag}, \text{Rh}, \text{Cu}, \text{Pt}, \text{Ru}, \text{Ni}, \text{Ir}, \text{Pd},$ and Co) catalysts has a volcano-shaped dependence on the d -band center.⁴⁸ The relationship of H_2 production rate from ethanol reforming with d -band center has a volcano-shaped curve over the M/TiO_2 ($\text{M} = \text{Au}, \text{Pd},$ and Pt).⁴⁹

4.3. Influences of Surface Termination and Supported Metal Types on the Selectivity of CH_x Intermediate Based on Microkinetic Modeling. During the process of CH_x ($x = 1-3$) generation, the intermediates CH_xOH ($x = 1, 2$) and CH_xO ($x = 1-3$) may undergo hydrogenation to produce unwanted CH_3OH , which could decrease the selectivity of CH_x ($x = 1-3$) intermediate. As shown in Figure 6b, the WC-W, Cu/WC-C, and Rh/WC-C catalysts prefer the generation of the abundant CH_x monomer, in which CH_3OH can be effectively inhibited. Correspondingly, the selectivity of CH is 99.81, 100, and 60.47%, respectively (Table S4). However, the Cu/WC-W and Rh/WC-W catalysts dominantly contribute to CH_3OH production; correspondingly, CH_3OH selectivity is 93.35 and 98.78% (Table S4). The above results show that the surface termination and supported metal types in the M/WC ($\text{M} = \text{Cu}$ or Rh) catalysts greatly alter the selectivity of CH_x ($x = 1-3$) and CH_3OH ; more importantly, the C-termination in the $\text{M}/\text{WC-C}$ ($\text{M} = \text{Cu}$ or Rh) catalysts could effectively inhibit CH_3OH production compared to the W-termination.

4.4. Electronic Properties of $\text{M}/\text{WC-C}$ ($\text{M} = \text{Cu}$ or Rh) with Noble Metal-Like Character. As mentioned above, the C-termination in the $\text{M}/\text{WC-C}$ ($\text{M} = \text{Cu}$ or Rh) catalysts could effectively inhibit CH_3OH production compared to the W-termination, which could be attributed to the formation of metal carbide consisted of the monolayer Cu/Rh with the C-termination of WC in the $\text{M}/\text{WC-C}$ ($\text{M} = \text{Cu}$ or Rh) catalysts, facilitating the rupture of C-O bond. For example, the formation of Cu_xC significantly improves the activity of acetylene hydrogenation over the Cu_2O nanocubes catalyst.⁵⁰ The production of RhC_x enhances the activity and selectivity of ethanol from syngas conversion over RhMn/SiO_2 catalyst, in which CH_x is easily produced.⁵¹ $\gamma\text{-Fe}_5\text{C}_2(001)$ with Fe-

termination favors CO direct conversion to C and O atoms, which performs the great activity toward the FTS reaction.⁵²

To analyze the bond nature between the surface M ($\text{M} = \text{Cu}$ or Rh) atoms and the subsurface C atoms in the $\text{M}/\text{WC-C}$ ($\text{M} = \text{Cu}$ or Rh) catalysts, the electron location function (ELF) is carried out.⁵³ As shown in Figure 8a, the ELF of the M/

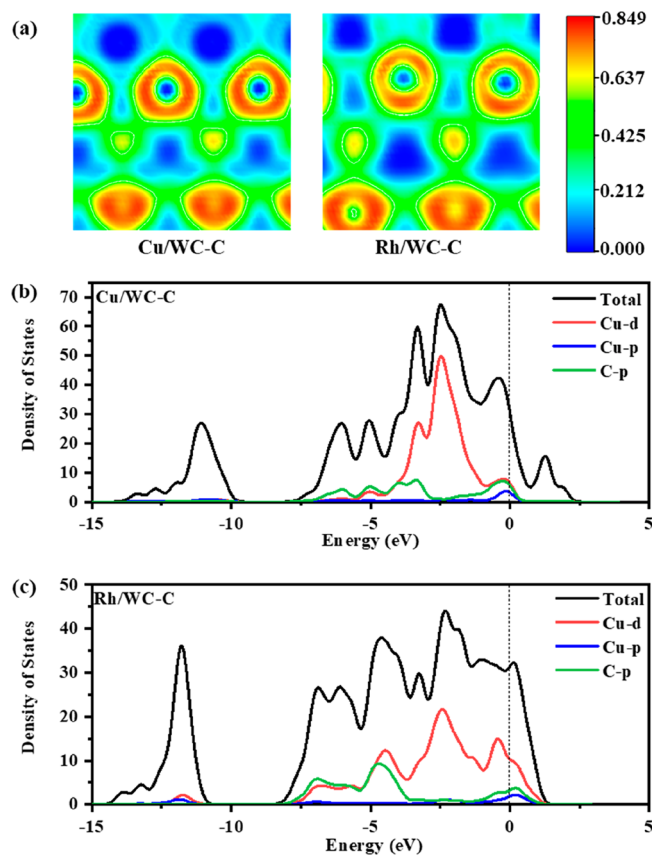


Figure 8. (a) Electrons location function (ELF) for the M-C ($\text{M} = \text{Rh}/\text{Cu}$) bonds in the Cu/WC-C and Rh/WC-C catalysts. Density of states (DOS) consisting of surface Cu/Rh atoms and subsurface C atoms in the (b) Cu/WC-C and (c) Rh/WC-C catalysts.

WC-C ($\text{M} = \text{Cu}$ or Rh) catalysts is presented by slicing planes along the M-C ($\text{M} = \text{Cu}$ or Rh) bonds, indicating that the bond of the subsurface C atom and the surface M ($\text{M} = \text{Cu}$ or Rh) atoms presents the metallic bond characteristic in the $\text{M}/\text{WC-C}$ ($\text{M} = \text{Cu}$ or Rh) catalysts; furthermore, as shown in Figure 8b,c, the DOS consisted of surface M ($\text{M} = \text{Cu}$ or Rh) atoms and the subsurface C atoms showed that there is no band gap near the Fermi level.

Thus, the formation of metal carbide consisted of the monolayer Cu/Rh with the C-termination of WC in the $\text{M}/\text{WC-C}$ ($\text{M} = \text{Cu}$ or Rh) catalysts greatly enhance the catalytic performance toward the abundant CH_x ($x = 1-3$) monomer, as well as significantly inhibit CH_3OH generation. Cu/WC-C presents the highest CH activity than WC-W, and the essential reason is attributed to the formation of the unique CuC_x structure, which exhibits the special activity toward CO direct dissociation to facilitate CH formation.

4.5. Influences of the Temperature and H_2/CO Ratio on the CH_x ($x = 1-3$) and CH_3OH Production.

4.5.1. Influences of the Temperature. Reaction temperature has a significant influence on the catalytic performance of

syngas conversion to produce CH_x ($x = 1-3$) and CH_3OH .^{1,54} Since this process often takes place at 500–623 K,^{2,25} the temperatures of 500, 523, 550, 573, 600, and 623 K are carried out. As shown in Figure 9a–e and Table S5, over the WC–W and M/WC ($M = \text{Cu}$ or Rh) catalysts, the rate of CH_x ($x = 1-3$) and CH_3OH generation gradually increase with the increasing temperature.

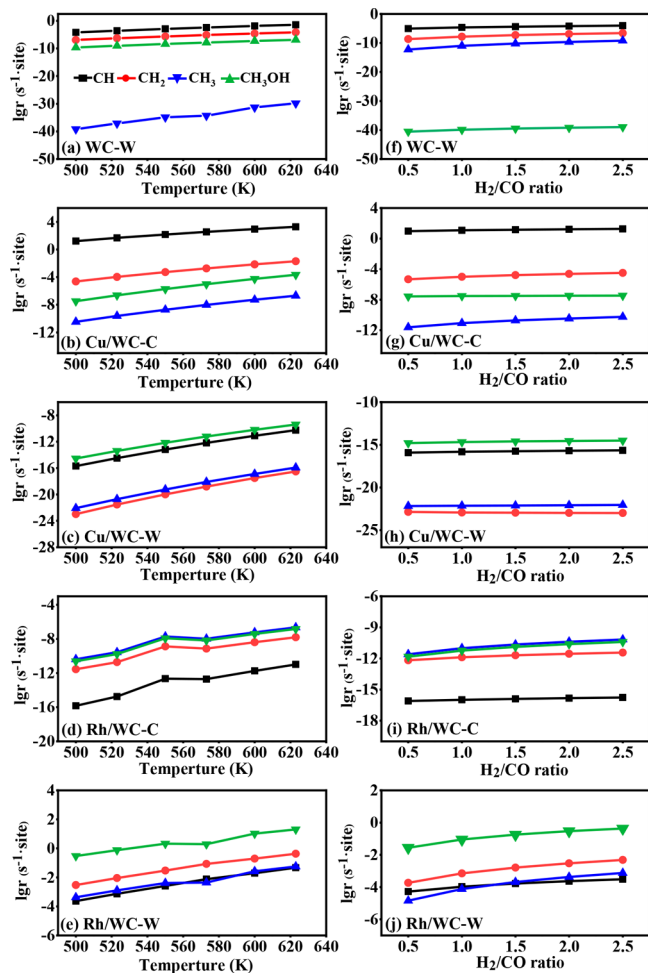


Figure 9. Rate change trend of CH_x ($x = 1-3$) and CH_3OH production with the temperature increasing (a–e) and the H_2/CO ratio increasing (f–j) over the WC–W, Cu/WC–C, Cu/WC–W, Rh/WC–C, and Rh/WC–W catalysts.

Over the WC–W, Cu–WC–C, and Rh–WC–C catalysts, as presented in Figure 9a,b,d, CH_x ($x = 1-3$) generation rates are still higher than CH_3OH generation rates with the temperature increasing, resulting in high CH_x ($x = 1-3$) selectivity. Meanwhile, over the WC–W and Cu/WC–C catalysts, the increasing degree of CH rate is similar to that of CH_3OH rate, so the selectivity of CH (99.81 and 100%) and CH_3OH (0%) remained unchanged. However, over Rh/WC–C, the increasing degree of CH_3 rate is slightly slower than that of CH_3OH rate, resulting in the increasing of CH_3OH selectivity (35.42, 35.98, 36.57, 37.03, 37.51, and 37.89%). As shown in Figure 9c,e as well as Table S5, CH_x ($x = 1-3$) generation rates are still lower than CH_3OH generation rates with increasing temperature, resulting in high CH_3OH selectivity. Over Cu/WC–W, the increasing degree of CH_2 rate is quicker than that of CH_3OH rate with the temperature

increasing, which decreases CH_3OH selectivity (93.35, 92.40, 91.23, 90.18, 88.90, and 87.78%). Over Rh/WC–W, the increasing degree of CH_2 rate is slightly quicker than that of CH_3OH rate at first with the temperature increasing and then lower than that of CH_3OH , which decreases CH_3OH selectivity at first and then increases CH_3OH selectivity (98.78, 98.57, 98.28, 95.27, 97.72, and 97.41%).

Above analysis shows that the reaction temperature greatly impacts the catalytic performance toward CH_x ($x = 1-3$) and CH_3OH generation over the M/WC ($M = \text{Cu}$ or Rh). The temperatures of 623, 500, and 573 K are the most suitable to inhibit CH_3OH production over the Cu/WC–W, Rh/WC–C, and Rh/WC–W, respectively.

4.5.2. Influences of the H_2/CO Ratio on CH_x ($x = 1-3$) and CH_3OH Production. The H_2/CO ratios in syngas also impact the catalytic performance, so the H_2/CO ratio from 0.45 to 3 is adopted in experiment.⁵⁵ In this study, the H_2/CO ratio focuses on 0.5, 1, 1.5, 2, and 2.5. As shown in Figure 9f,g,i as well as Table S6, CH_x ($x = 1-3$) generation rates over the WC–W, Cu/WC–C, and Rh/WC–C catalysts are still higher than the CH_3OH generation rates, resulting in high CH_x ($x = 1-3$) selectivity with increasing H_2/CO ratio. Meanwhile, over the WC–W and Cu/WC–C catalysts, the increasing degree of CH rate is similar to that of the CH_3OH rate with the increasing H_2/CO ratio. Thus, CH_3OH selectivity (0%) remained unchanged, whereas the increasing degree of CH_3 rate over Rh/WC–C is lower than that of CH_3OH rate, which increase CH_3OH selectivity with the increasing H_2/CO ratio (31.51, 34.01, 34.94, 35.42, and 35.73%).

As shown in Figure 9h,j as well as Table S6, the rate of CH_3OH generation is still higher in comparison with that of CH_x ($x = 1-3$) monomers, resulting in high CH_3OH selectivity with increasing H_2/CO ratio over the Cu/WC–W and Rh/WC–W catalysts. Meanwhile, over Cu/WC–W, the increasing degree of CH rate is lower than that of CH_3OH rate with the H_2/CO ratio increasing, so CH_3OH selectivity increases (92.95, 93.17, 93.28, 93.35, and 93.40%). Over Rh/WC–W, the increasing degree of CH_2 rate is slightly quicker than that of CH_3OH rate with the increasing H_2/CO ratio, which slightly decreases CH_3OH selectivity (99.10, 99.02, 98.90, 98.78, and 98.65%).

Thus, the H_2/CO ratio affects the catalytic performance toward the generation of CH_x ($x = 1-3$) and CH_3OH over the WC–C and M/WC ($M = \text{Cu}$ or Rh) catalysts. The H_2/CO ratios of 0.5, 0.5, and 2.5 are the most suitable to inhibit CH_3OH over the Cu/WC–W, Rh/WC–C, and Rh/WC–W, respectively.

4.6. Influences of Surface Termination and Supported Metal Types on C_2 Species. Once the CH_x ($x = 1-3$) intermediate was generated, its related reactions easily occur, including CH_x hydrogenation to CH_4 , CH_x reacting with CO to CH_xCO , and CH_x ($x = 1-3$) self-coupling.⁵⁶ Since CH_3OH generation over the WC–W, Cu/WC–C, and Rh/WC–C catalysts could be inhibited, leading to great CH_x ($x = 1-3$) selectivity. However, the Cu/WC–W and Rh/WC–W catalysts prefer CH_3OH generation rather than CH_x ($x = 1-3$), resulting in the difficult production of C_2 species. For the Cu/WC and Rh/WC catalysts, the C-termination of WC contributes to C_2 species generation, while the W-termination is only preferable for CH_3OH generation. Thus, starting from CH, CH_2 , and CH_3 , the generation of methane and C_2 species over the WC–W, Cu/WC–C, and Rh/WC–C catalysts are considered to identify the most suitable catalyst toward C_2

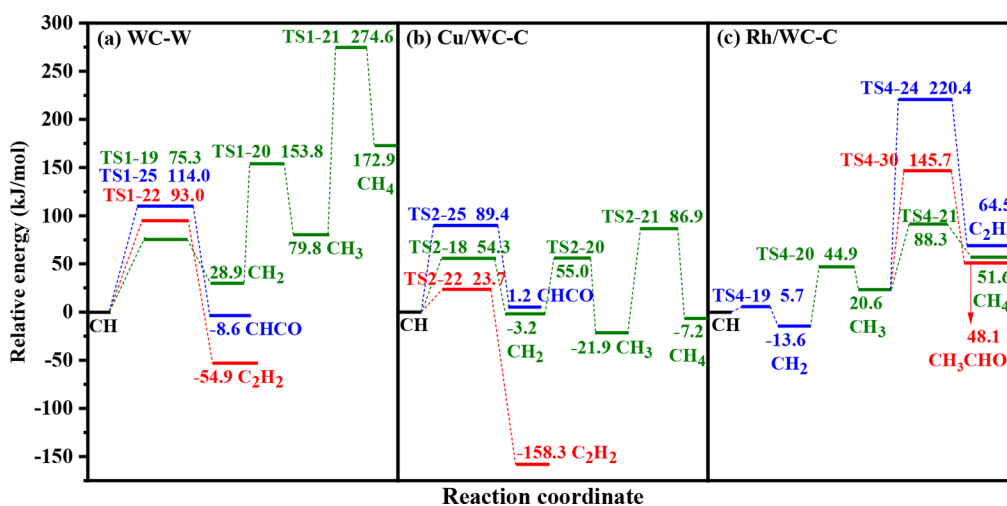


Figure 10. Free energy profiles for the generation of methane, the preferred C_2 oxygenate precursor and C_2 hydrocarbons over the (a) WC-W, (b) Cu/WC-C, and (c) Rh/WC-C catalysts.

species generation (see the details in the [Supporting Information](#)). **Figure 10** only presents the overall barriers of methane, the abundant C_2 oxygenate precursor and C_2 hydrocarbon.

As presented in **Figure 10**, over WC-W, the overall barriers of C_2 oxygenate precursor (CHCO), methane, and C_2 hydrocarbon (C_2H_2) are 114.0, 274.6, and 93.0 $\text{kJ}\cdot\text{mol}^{-1}$, respectively, which shows that C_2 hydrocarbon C_2H_2 is the abundant product. Over Cu/WC-C, the overall barriers of C_2 oxygenate precursor (CHCO), methane, and C_2 hydrocarbon (C_2H_2) are 89.4, 86.9, and 23.7 $\text{kJ}\cdot\text{mol}^{-1}$, respectively, so C_2 hydrocarbon C_2H_2 is the dominant product. On Cu(111), CH_3OH generation more easily occurs in comparison with CH_x ($x = 1-3$) generation, resulting in the abundant product CH_3OH instead of C_2 species, so the WC support in Cu/WC-C catalyst alters the type of main product. Over Rh/WC-C, the overall barriers of C_2 oxygenate precursor, methane, and C_2 hydrocarbon are 145.7, 88.3, and 220.4 $\text{kJ}\cdot\text{mol}^{-1}$, respectively, which indicates that the product primarily focus on methane. However, on Rh(111),⁴¹ the main product is CHCHO rather than methane; thus, the WC support in Rh/WC-C catalyst also changes the type of dominant product.

The above analysis indicates that the abundant product over Rh/WC-C is methane; however, the WC-W and Cu/WC-C catalysts mainly contribute to the generation of C_2 species. Among these, the Cu/WC-C catalyst not only gives an excellent activity and selectivity toward CH_x ($x = 1-3$) to provide the abundant CH_x for C_2 species but also shows high activity for C_2H_2 generation starting from the abundant CH_x monomer. Moreover, Cu/WC-C catalyst could be experimentally prepared. For example, Yao et al.⁵⁷ synthesized Cu/WC catalyst, in which Cu/CF(Cu foam) was first obtained by a wet chemical method and an electrochemical method, and then the WC layer was directly deposited onto Cu/CF by the process of magnetron sputtering. Kelly et al.⁵⁸ prepared Rh/WC catalyst via the physical vapor deposition; specifically, the Rh wire was heated under a desirable temperature to evaporate Rh atoms onto WC catalyst. Meanwhile, the coverage of Rh atoms was estimated using the Rh/W AES peak intensity ratio. Liu et al.¹² prepared Rh/W_xC catalyst by the method of incipient wetness impregnation; it was dried at 383 K for 3 h,

and then reduced under H_2 flow at 723 K, using a temperature ramp of 1 $\text{K}\cdot\text{min}^{-1}$.

However, based on the previous studies,^{59,60} the generation rates of CH_4 , C_2 hydrocarbons, and C_2 oxygenate precursor (r_{CH_4} , $r_{CH_i+CH_j}$ and $r_{CH_i+CO/CHO}$) can be expressed by eqs 2–4, respectively (see details in the [Supporting Information](#)).

$$\begin{aligned} r_{CH_4} &= A e^{-E_a^{hy}/RT} \theta_{CH_3} \theta_H \\ &= A e^{-E_a^{hy} + E_3/RT} t^3 \theta_C \theta_H \\ &= A e^{-E_{\text{eff},CH_4}/RT} t^3 \theta_C \theta_H \end{aligned} \quad (2)$$

$$\begin{aligned} r_{CH_i+CH_j} &= A e^{-E_a^{ij}/RT} \theta_{CH_i} \theta_{CH_j} \\ &= A e^{-E_a^{ij} + E_i + E_j/RT} t^{i+j} \theta_C^2 \\ &= A e^{-E_{\text{eff},CH_i+CH_j}/RT} t^{i+j} \theta_C^2 \end{aligned} \quad (3)$$

$$\begin{aligned} r_{CH_i+CO/CHO} &= A e^{-E_a^{i,CO/CHO}/RT} \theta_{CH_i} \theta_{CO/CHO} \\ &= A e^{-E_a^{i,CO/CHO} + E_i/RT} t^i \theta_C \theta_{CO/CHO} \\ &= A e^{-E_{\text{eff},CH_i+CO/CHO}/RT} t^i \theta_C \theta_{CO/CHO} \end{aligned} \quad (4)$$

According to above equations, the ratio for the rate of C_2H_x (C_2H_xO) generation to that of CH_4 generation, as well as the ratio for the rate of C_2H_x generation to that of C_2H_xO generation can be expressed by eqs 5–7, respectively.^{59,60}

$$\frac{r_{C_2H_x}}{r_{CH_4}} = e^{-\Delta E_{\text{eff}}(C_2H_x-CH_4)/RT} \times X \quad (5)$$

$$\frac{r_{C_2H_xO}}{r_{CH_4}} = e^{-\Delta E_{\text{eff}}(C_2H_xO-CH_4)/RT} \times X \quad (6)$$

$$\frac{r_{C_2H_x}}{r_{C_2H_xO}} = e^{-\Delta E_{\text{eff}}(C_2H_x-C_2H_xO)/RT} \times X \quad (7)$$

$$X = t^{(i+j)-i} \theta_C / \theta_{CO} \quad (8)$$

where $\Delta E_{\text{eff}}(C_2H_x - CH_4)$ and $\Delta E_{\text{eff}}(C_2H_xO - CH_4)$ are the effective barrier differences between C_2H_x (C_2H_xO) and CH_4 generation and $\Delta E_{\text{eff}}(C_2H_x - C_2H_xO)$ represents that between C_2H_x and C_2H_xO generation. More importantly, the

ratio for the rate of C_2H_x (C_2H_xO) generation to that of CH_4 generation, as well as the ratio for the rate of C_2H_x generation to that of C_2H_xO generation are greatly impacted by ΔE_{eff} owing to its exponential influence, suggesting that ΔE_{eff} put a greater influence in comparison with θ_C/θ_{CO} and t . Thus, C_2 species selectivity could be reflected by the effective barrier difference (ΔE_{eff}). Moreover, when the value of E_{eff} for C_2 species is lower than that of methane, this leads to a negative value of ΔE_{eff} and high C_2 species selectivity. Conversely, the positive value of ΔE_{eff} means the low C_2 species selectivity.

As in Table S7, the values of E_{eff} (C_2H_2) are smaller than those of E_{eff} (CH_4) and E_{eff} ($CHCO$) over the WC–W (–120.4 vs 236.0 and 7.3 $\text{kJ}\cdot\text{mol}^{-1}$) and Cu/WC–C (–156.1 vs 226.1 and –0.5 $\text{kJ}\cdot\text{mol}^{-1}$), suggesting that the product dominantly focuses on C_2 hydrocarbons C_2H_2 . The values of E_{eff} (CH_4) are smaller than those of E_{eff} (C_2H_6) and E_{eff} (CH_3CHO) on Rh/WC–C (153.6 vs 371.6 and 211.0 $\text{kJ}\cdot\text{mol}^{-1}$); namely, the main product is CH_4 , which agrees with the results based on the activation barrier.

However, ΔE_{eff} ($CHCO-CH_4$), ΔE_{eff} ($C_2H_2-CH_4$), and ΔE_{eff} (C_2H_2-CHCO) on the WC–W catalyst (Table S7) are –228.7, –356.4, and –127.7 $\text{kJ}\cdot\text{mol}^{-1}$, respectively; namely, the WC–W catalyst dominantly contributes to the production of C_2H_2 hydrocarbon rather than $CHCO$ and CH_4 . The same thing also occurs on Cu/WC–C catalyst, and C_2H_2 hydrocarbon is the dominant product. However, ΔE_{eff} ($CH_3CHO-CH_4$) and ΔE_{eff} ($C_2H_6-CH_4$) on the Rh/WC–C catalyst are 57.4 and 218.0 $\text{kJ}\cdot\text{mol}^{-1}$, respectively; namely, the Rh/WC–C catalyst mainly contributes to the generation of CH_4 instead of C_2 species. Thus, only the Cu/WC–C catalyst exhibits outstanding selectivity of C_2H_2 .

The above analysis shows the surface termination and supported metal types in the M/WC–C ($M = \text{Cu}$ or Rh) catalyst can alter catalytic performance toward CH_x ($x = 1-3$), CH_3OH , as well as C_2 species produced from syngas. In particular, the Cu/WC–C catalyst is screened out to exhibit the highest activity toward CH_x ($x = 1-3$) generation, which is caused by the moderate d -band center; moreover, the greater effective barrier difference is dominantly responsible for the generation of C–C chain to perform the outstanding catalytic performance toward C_2 species generation over Cu/WC–C catalyst. Thus, the catalytic performance of the WC-supported metal monolayer depends on their exposed termination, which provides a valuable clue for rationally constructing the metal catalyst supported over the transition metal carbides to achieve the outstanding catalytic performance in the conversion of syngas to C_2 species.

4.7. Comparisons of the Reported Results with Our Results over the WC and M/WC ($M = \text{Rh}$, Cu). Griboval-Constant et al.⁶¹ found that WC catalyst is responsible for generation of light alkanes (C_1-C_4 selectivity: 78%) and heavier alkanes (C_{5+} selectivity: 22%) from syngas conversion, with no alcohol production. Christensen et al.⁶² also found WC catalyst promoted by K_2CO_3 mainly produced alkane at 649 K. Meanwhile, the catalytic performance of WC catalyst is similar to Mo_2C catalyst for syngas conversion.⁶³ Xiang et al.⁶⁴ reported that hydrocarbons are main product over Mo_2C catalyst in syngas conversion. Zhang et al.⁶⁵ found that CH_3OH is main product over the Rh/ W_2C catalyst in syngas conversion. These results directly and indirectly supported our obtained result that the WC catalyst is responsible for light alkane generation and the Rh/WC–W catalyst mainly generates CH_3OH .

Furthermore, our results also show that the Cu/WC–C and Cu/WC–W catalysts perform the higher CO activation ability compared with the WC–W catalyst; namely, the synergistic effect of WC support and Cu atoms in the Cu/WC–C and Cu/WC–W catalysts are responsible for the higher CO activation ability. This result is well-supported by the previously experimental and theoretical results. For example, Rodriguez et al.⁶⁶ experimentally found that Cu/TiC catalyst usually exhibits superior activity for CO_2 reduction to CO compared with the pure TiC catalyst. Posada-Pérez et al.³³ studied CH_3OH generation from CO_2 hydrogenation over Cu/ δ -MoC catalyst, suggesting that CH_3OH generation requires the apparent activation energy lower than that of δ -MoC catalyst at 550 K; more importantly, CO serves as a key intermediate in the process of CO_2 hydrogenation to CH_3OH , which indicates that CO is easily activated over Cu/ δ -MoC catalyst. Cu/ δ -MoC catalyst could present the high ability of CO conversion. Similarly, Koverga et al.⁶⁷ theoretically reported that Cu/WC–W catalyst performs the higher ability of CO_2 activation than WC–W catalyst.

5. CONCLUSIONS

In this work, the underlying function of surface termination and supported metal types in the catalysts with the Cu or Rh supported over WC (M/WC ($M = \text{Cu}$ or Rh)) for the generation of C_2 species from syngas is examined by DFT calculations and microkinetic modeling. The WC–W, Cu/WC–C, Cu/WC–W, Rh/WC–C, and Rh/WC–W catalysts perform the great stability evaluated using AIMD simulations. The surface termination and supported metal types alter the dominant existence of abundant CH_x monomer; specifically, the abundant CH_x monomer is CH over WC–W, Cu/WC–C, and Cu/WC–W, CH_3 over Rh/WC–C, and CH_2 over Rh/WC–W. Among these, the Cu/WC–C catalyst shows the highest activity of CH generation due to the moderate d -band center. The WC–W, Cu/WC–C, and Rh/WC–C catalysts could effectively inhibit CH_3OH generation with high CH_x ($x = 1, 3$) selectivity. Subsequently, only the WC–W and Cu/WC–C catalysts can contribute to C_2 species generation, while Rh/WC–C is responsible for CH_4 generation. Among five kinds of catalysts, the Cu/WC–C catalyst is screened out to exhibit outstanding activity and selectivity toward the generation of C_2 species. Therefore, the surface termination and supported metal types in the M/WC ($M = \text{Cu}$ or Rh) catalysts are the key structure information to determine the catalytic performance, which can be used as an effective way for rationally constructing the non-noble metal catalyst to generate C_2 species with excellent activity and selectivity in syngas conversion.

■ ASSOCIATED CONTENT

Supporting Information

The Supporting Information is available free of charge at <https://pubs.acs.org/doi/10.1021/acsami.2c02217>.

Detailed descriptions about the calculations of adsorption energy and the most stable configurations of related species, H_2 adsorption and dissociation, as well as the generation of CH_x ($x = 1-3$) and CH_3OH , analysis of electronic properties, microkinetic modeling, the production of C_2 species, as well as the effective barrier (PDF)

AUTHOR INFORMATION

Corresponding Authors

Baojun Wang – College of Chemical Engineering and Technology, Taiyuan University of Technology, Taiyuan, Shanxi 030024, PR China; State Key Laboratory of Clean and Efficient Coal Utilization, Taiyuan University of Technology, Taiyuan, Shanxi 030024, PR China; Key Laboratory of Coal Science and Technology, Taiyuan University of Technology, Ministry of Education, Taiyuan, Shanxi 030024, PR China; orcid.org/0000-0002-9069-6720; Email: wangbaojun@tyut.edu.cn

Riguang Zhang – State Key Laboratory of Clean and Efficient Coal Utilization, Taiyuan University of Technology, Taiyuan, Shanxi 030024, PR China; Key Laboratory of Coal Science and Technology, Taiyuan University of Technology, Ministry of Education, Taiyuan, Shanxi 030024, PR China; orcid.org/0000-0001-8956-8425; Email: zhangriguang@tyut.edu.cn

Authors

Wantong Zhao – College of Chemical Engineering and Technology, Taiyuan University of Technology, Taiyuan, Shanxi 030024, PR China; State Key Laboratory of Clean and Efficient Coal Utilization, Taiyuan University of Technology, Taiyuan, Shanxi 030024, PR China

Zun Guan – College of Chemical Engineering and Technology, Taiyuan University of Technology, Taiyuan, Shanxi 030024, PR China; State Key Laboratory of Clean and Efficient Coal Utilization, Taiyuan University of Technology, Taiyuan, Shanxi 030024, PR China

Debao Li – State Key Laboratory of Coal Conversion, Institute of Coal Chemistry, Chinese Academy of Sciences, Taiyuan, Shanxi 030001, PR China; orcid.org/0000-0002-6891-4787

Maohong Fan – College of Engineering and Applied Science, University of Wyoming, Laramie, Wyoming 82071, United States; School of Civil and Environmental Engineering, Georgia Institute of Technology, Atlanta, Georgia 30332, United States; School of Energy Resources, University of Wyoming, Laramie, Wyoming 82071, United States; orcid.org/0000-0003-1334-7292

Complete contact information is available at: <https://pubs.acs.org/10.1021/acsami.2c02217>

Notes

The authors declare no competing financial interest.

ACKNOWLEDGMENTS

This work is financially supported by Key Projects of National Natural Science Foundation of China (No. 21736007), National Natural Science Foundation of China (No. 22078221) and Science Foundation for Distinguished Young Scholar of Shanxi Province (No. 20210302121005).

REFERENCES

- (1) Ao, M.; Pham, G. H.; Sunarso, J.; Tade, M. O.; Liu, S. M. Active Centers of Catalysts for Higher Alcohol Synthesis from Syngas: A Review. *ACS Catal.* **2018**, *8*, 7025–7050.
- (2) Spivey, J. J.; Egbeki, A. Heterogeneous Catalytic Synthesis of Ethanol from Biomass-derived Syngas. *Chem. Soc. Rev.* **2007**, *36*, 1514–1528.
- (3) Sun, X. C.; Zhang, R. G.; Wang, B. J. Insights into the Preference of CH_x ($x = 1-3$) Formation from CO Hydrogenation on Cu(111) Surface. *Appl. Surf. Sci.* **2013**, *265*, 720–730.
- (4) Zheng, H. Y.; Zhang, R. G.; Li, Z.; Wang, B. J. Insight into the Mechanism and Possibility of Ethanol Formation from Syngas on Cu(100) Surface. *J. Mol. Catal. A-Chem.* **2015**, *404-405*, 115–130.
- (5) Zhang, R. G.; Sun, X. C.; Wang, B. J. Insight into the Preference Mechanism of CH_x ($x = 1-3$) and C–C Chain Formation Involved in C_2 Oxygenate Formation from Syngas on the Cu(110) Surface. *J. Phys. Chem. C* **2013**, *117*, 6594–6606.
- (6) Brungs, A. J.; York, A. P. E.; Green, M. L. H. Comparison of the Group V and VI Transition Metal Carbides for Methane Dry Reforming and Thermodynamic Prediction of Their Relative Stabilities. *Catal. Lett.* **1999**, *57*, 65–69.
- (7) Won, B. D.; Jeong, M. H.; Kim, M. H.; Chung, C. H.; Moon, D. J.; Suh, Y. W.; Baik, J. H.; Bae, J. W. Rh-Mn/tungsten Carbides for Direct Synthesis of Mixed Alcohols from Syngas: Effects of Tungsten Carbide Phases. *Micropor. Mesopor. Mater.* **2018**, *255*, 44–52.
- (8) Zhang, R. G.; Wei, C.; Guo, W. S.; Li, Z. Q.; Wang, B. J.; Ling, L. X.; Li, D. B. Syngas Conversion to C_2 Oxygenates over Cu/ β - Mo_2C Catalyst: Probing into the Effect of the Interface between Cu and β - Mo_2C on Catalytic Performance. *J. Phys. Chem. C* **2019**, *123*, 21022–21030.
- (9) Liang, Y.; Chen, L.; Ma, C. Kinetics and Thermodynamics of H_2O Dissociation and CO Oxidation on the Pt/WC (0001) Surface: A Density Functional Theory Study. *Surf. Sci.* **2017**, *656*, 7–16.
- (10) Zhang, X.; Lu, Z.; Yang, Z. A Theoretical Understanding on the CO-tolerance Mechanism of the WC(0001) Supported Pt Monolayer: Some Improvement Strategies. *Appl. Surf. Sci.* **2016**, *389*, 455–461.
- (11) Cui, G.; Shen, P. K.; Meng, H.; Zhao, J.; Wu, G. Tungsten Carbide as Supports for Pt Electrocatalysts with Improved CO Tolerance in Methanol Oxidation. *J. Power Sources* **2011**, *196*, 6125–6130.
- (12) Liu, Y. F.; Zhang, L. F.; Göltl, F.; Ball, M. R.; Hermans, I.; Kuech, T. F.; Mavrikakis, M.; Dumesic, J. A. Synthesis Gas Conversion over Rh-Mn-W_xC/SiO₂ Catalysts Prepared by Atomic Layer Deposition. *ACS Catal.* **2018**, *8*, 10707–10720.
- (13) Rao, X. F.; Lou, Y. T.; Zhou, Y.; Zhang, J. B.; Zhong, S. W. First-principles Insights into Ammonia Decomposition on WC (0001) Surface Terminated by W and C. *Appl. Surf. Sci.* **2021**, *566*, 150635.
- (14) Zheng, W. F.; Chen, L. T.; Ma, C. A Density Functional Study of H_2O Adsorption and Dissociation on WC(0001). *Comput. Theor. Chem.* **2014**, *1039*, 75–80.
- (15) Hwu, H. H.; Polizzotti, B. D.; Chen, J. G. G. Potential Application of Tungsten Carbides as Electrocatalysts. 2. Coadsorption of CO and H_2O on Carbide-modified W(111). *J. Phys. Chem. B* **2001**, *105*, 10045–10053.
- (16) Koverga, A. A.; Flórez, E.; Dorkis, L.; Rodriguez, J. A. CO, CO₂, and H₂ Interactions with (0001) and (001) Tungsten Carbide Surfaces: Importance of Carbon and Metal sites. *J. Phys. Chem. C* **2019**, *123*, 8871–8883.
- (17) Vasic, D. D.; Pasti, I. A.; Mentus, S. V. DFT Study of Platinum and Palladium Overlayers on Tungsten Carbide: Structure and Electrocatalytic Activity toward Hydrogen Oxidation/evolution Reaction. *Int. J. Hydrogen Energy* **2013**, *38*, 5009–5018.
- (18) Perdew, J. P.; Burke, K.; Ernzerhof, M. Generalized Gradient Approximation Made Simple. *Phys. Rev. Lett.* **1996**, *77*, 3865–3868.
- (19) Kresse, G.; Furthmüller, J. Efficient Iterative Schemes for Ab Initio Total-energy Calculations Using a Plane-wave Basis Set. *Phys. Rev. B* **1996**, *54*, 11169–11186.
- (20) Monkhorst, H. J.; Pack, J. D. Special Points for Brillouin-zone Integrations. *Phys. Rev. B* **1976**, *13*, 5188–5192.
- (21) Henkelman, G.; Uberuaga, B. P.; Jónsson, H. A Climbing Image Nudged Elastic Band Method for Finding Saddle Points and Minimum Energy Paths. *J. Chem. Phys.* **2000**, *113*, 9901–9904.
- (22) Olsen, R. A.; Kroes, G. J.; Henkelman, G.; Arnaldsson, A.; Jonsson, H. Comparison of Methods for Finding Saddle Points

without Knowledge of the Final States. *J. Chem. Phys.* **2004**, *121*, 9776–9792.

(23) Zhang, X. L.; Yang, Z. X.; Wu, R. Q. A Au Monolayer on WC(0001) with Unexpected High Activity towards CO Oxidation. *Nanoscale* **2018**, *10*, 4753.

(24) Ma, C. A.; Liu, T.; Chen, L. T. A Computational Study of H₂ Dissociation and CO Adsorption on the Pt_{ML}/WC(0001) Surface. *Appl. Surf. Sci.* **2010**, *256*, 7400–7405.

(25) Zhang, R. G.; Liu, F.; Wang, B. J. Co-decorated Cu Alloy Catalyst for C₂ Oxygenate and Ethanol Formation from Syngas on Cu-based Catalyst: Insight into the Role of Co and Cu as well as the Improved Selectivity. *Catal. Sci. Technol.* **2016**, *6*, 8036–8054.

(26) Zhang, B.; Lin, Z.; Dong, H.; Wang, L. W.; Pan, F. Revealing Cooperative Li-ion Migration in Li_{1+x}Al_xTi_{2-x}(PO₄)₃ Solid State Electrolytes with High Al Doping. *J. Mater. Chem. A* **2020**, *8*, 342–348.

(27) Saeed, M. H.; Ahmed, S.; Muhammad, I.; Murtaza, I.; Ghani, A.; Ali, A.; Abdullah, R.; Wasif-ur-Rehman; Junaid-ur-Rehman; Khaliq, A. Molybdenum Carbide Nano-sheet as a High Capacity Anode Material for Monovalent Alkali Metal-ion Batteries-theoretical Investigation. *Phys. Lett. A* **2020**, *384*, 126688.

(28) Li, S. L.; Yam, K. M.; Guo, N.; Zhao, Y.; Zhang, C. Highly Stable Two-dimensional Metal-carbon Monolayer with Interpenetrating Honeycomb Structures. *npj 2D Mater. Appl.* **2021**, *5*, 52.

(29) Su, Y. Q.; Wang, Y. F.; Liu, J. X.; Filot, I. A. W.; Alexopoulos, K.; Zhang, L.; Muravev, V.; Zijlstra, B.; Vlachos, D. G.; Hensen, E. J. M. Theoretical Approach to Predict the Stability of Supported Single-atom Catalysts. *ACS Catal.* **2019**, *9*, 3289–3297.

(30) Chen, X.; Hu, R. DFT-based Study of Single Transition Metal Atom Doped g-C₃N₄ as Alternative Oxygen Reduction Reaction Catalysts. *Int. J. Hydrogen Energy* **2019**, *44*, 15409–15416.

(31) Chhina, H.; Campbell, S.; Kesler, O. Thermal and Electrochemical Stability of Tungsten Carbide Catalyst Supports. *J. Power Sources* **2007**, *164*, 431–440.

(32) Vidal, A. B.; Feria, L.; Evans, J.; Takahashi, Y.; Liu, P.; Nakamura, K.; Illas, F.; Rodriguez, J. A. CO₂ Activation and Methanol Synthesis on Novel Au/TiC and Cu/TiC Catalysts. *J. Phys. Chem. Lett.* **2012**, *3*, 2275–2280.

(33) Posada-Pérez, S.; Ramírez, P. J.; Evans, J.; Viñes, F.; Liu, P.; Illas, F.; Rodriguez, J. A. Highly Active Au/ δ -MoC and Cu/ δ -MoC Catalysts for the Conversion of CO₂: The Metal/C Ratio as a Key Factor Defining Activity, Selectivity, and Stability. *J. Am. Chem. Soc.* **2016**, *138*, 8269–8278.

(34) Kelly, T. G.; Stottleyer, A. L.; Ren, H.; Chen, J. G. Comparison of O-H, C-H, and C-O Bond Scission Sequence of Methanol on Tungsten Carbide Surfaces Modified by Ni, Rh, and Au. *J. Phys. Chem. C* **2011**, *115*, 6644–6650.

(35) Vasić Aničijević, D. D.; Nikolić, V. M.; Marčeta-Kaninski, M. P.; Pašti, I. A. Is Platinum Necessary for Efficient Hydrogen Evolution?—DFT Study of Metal Monolayers on Tungsten Carbide. *Int. J. Hydrogen Energy* **2013**, *38*, 16071–16079.

(36) Sun, X. T.; Yu, J. F.; Tong, X.; Yang, M.; Zhang, J. X.; Sun, J. Controlling Phase Transfer of Molybdenum Carbides by Various Metals for Highly Efficient Hydrogen Production. *J. Energy Chem.* **2021**, *62*, 191–197.

(37) Zhang, R. G.; Wang, G. R.; Wang, B. J. Insights into the Mechanism of Ethanol Formation from Syngas on Cu and an Expanded Prediction of Improved Cu-based Catalyst. *J. Catal.* **2013**, *305*, 238–255.

(38) Wei, C.; Zhang, R. G.; Ling, L. X.; Li, D. B.; Hou, B.; Wang, B. J. Syngas-to-C₂ Oxygenates on Cu-based Catalyst: Quantitative Insight into the Balancing Effect of Active Cu ^{δ} (0 ≤ δ ≤ 1) Sites. *Chem. Eng. Sci.* **2020**, *224*, 115785.

(39) Ren, H.; Chen, Y.; Huang, Y. L.; Deng, W. H.; Vlachos, D. G.; Chen, J. G. Tungsten Carbides as Selective Deoxygenation Catalysts: Experimental and Computational Studies of Converting C₃ Oxygenates to Propene. *Green Chem.* **2014**, *16*, 761–769.

(40) Kelly, T. G.; Chen, J. G. Controlling C-O, C-C and C-H Bond Scission for Deoxygenation, Reforming, and Dehydrogenation of

Ethanol using Metal-modified Molybdenum Carbide Surfaces. *Green Chem.* **2014**, *16*, 777–784.

(41) Kang, L.; Zhang, Y.; Ma, L. X.; Wang, B. J.; Fan, M. H.; Li, D. B.; Zhang, R. G. The Roles of Rh Crystal Phase and Facet in Syngas Conversion to Ethanol. *Chem. Eng. Sci.* **2022**, *248*, 117186.

(42) Raybaud, P.; Hafner, J.; Kresse, G.; Kasztelan, S.; Toulhoat, H. Structure, Energetics, and Electronic Properties of the Surface of a Promoted MoS₂ Catalyst: An Ab Initio Local Density Functional Study. *J. Catal.* **2000**, *190*, 128–143.

(43) Braga, A. A. C.; Caballero, A.; Urbano, J.; Diaz-Requejo, M. M.; Pérez, P. J.; Maseras, F. Mechanism of Side Reactions in Alkane C-H Bond Functionalization by Diazo Compounds Catalyzed by Ag and Cu Homoscorpionate Complexes—A DFT Study. *ChemCatChem.* **2011**, *3*, 1646–1652.

(44) Motagamwala, A. H.; Ball, M. R.; Dumesic, J. A. Microkinetic Analysis and Scaling Relations for Catalyst Design. *Annu. Rev. Chem. Biomol. Eng.* **2018**, *9*, 413–450.

(45) Andersson, M. P.; Dobberschütz, S.; Sand, K. K.; Tobler, D. J.; De Yoreo, J. J.; Stipp, S. L. S. A Microkinetic Model of Calcite Step Growth. *Angew. Chem., Int. Ed.* **2016**, *128*, 11252–11256.

(46) Zhang, Y. X.; Yang, Z. X. High Activity of Au Monolayer Doped by Pt Atom on WC(0001) Surface Towards H₂ Dissociation and High Tolerance of Sulfur Poisoning. *J. Alloys Compd.* **2019**, *775*, 330–334.

(47) Hunt, S. T.; Milina, M.; Alba-Rubio, A. C.; Hendon, C. H.; Dumesic, J. A.; Román-Leshkov, Y. Self-assembly of Noble Metal Monolayers on Transition Metal Carbide Nanoparticle Catalysts. *Science* **2016**, *352*, 974–978.

(48) Tamura, M.; Kon, K.; Satsuma, A.; Shimizu, K. Volcano-curves for Dehydrogenation of 2-propanol and Hydrogenation of Nitrobenzene by SiO₂-supported Metal Nanoparticles Catalysts as Described in terms of a *d*-band Model. *ACS Catal.* **2012**, *2*, 1904–1909.

(49) Al-Azri, Z. H. N.; Aloufi, M.; Chan, A.; Waterhouse, G. I. N.; Idriss, H. Metal Particle Size Effects on the Photocatalytic Hydrogen Ion Reduction. *ACS Catal.* **2019**, *9*, 3946–3958.

(50) Lu, C. Y.; Wang, Y.; Zhang, R. G.; Wang, B. J.; Wang, A. J. Preparation of an Unsupported Copper-based Catalyst for Selective Hydrogenation of Acetylene from Cu₂O Nanocubes. *ACS Appl. Mater. Interfaces* **2020**, *12*, 46027–46036.

(51) Huang, X.; Teschner, D.; Dimitrakopoulou, M.; Fedorov, A.; Frank, B.; Krahnert, R.; Rosowski, F.; Kaiser, H.; Schunk, S.; Kuretschka, C.; et al. Atomic-scale Observation of the Metal-promoter Interaction in Rh-based Syngas-upgrading Catalysts. *Angew. Chem., Int. Ed.* **2019**, *58*, 8709–8713.

(52) Ozbek, M. O.; Niemantsverdriet, J. W. Elementary Reactions of CO and H₂ on C-terminated γ -Fe₃C₂(001) Surfaces. *J. Catal.* **2014**, *317*, 158–166.

(53) Ma, Y. F.; Yu, G. T.; Wang, T.; Zhang, C. H.; Huang, X. R.; Chen, W. Highly Efficient Catalytic Activity for the Hydrogen Evolution Reaction on the Pristine and Monovacancy Defected WP Systems: A First-principles Investigation. *Phys. Chem. Chem. Phys.* **2018**, *20*, 13757–13764.

(54) Wang, J. J.; Zhang, Q. H.; Wang, Y. Rh-catalyzed Syngas Conversion to Ethanol: Studies on the Promoting Effect of FeO_x. *Catal. Today* **2011**, *171*, 257–265.

(55) Gupta, M.; Smith, M. L.; Spivey, J. J. Heterogeneous Catalytic Conversion of Dry Syngas to Ethanol and Higher Alcohols on Cu-Based Catalysts. *ACS Catal.* **2011**, *1*, 641–656.

(56) Zhang, R. G.; Kang, L.; Liu, H. X.; He, L. L.; Wang, B. J. Insight into the C-C Chain Growth in Fischer-Tropsch Synthesis on HCP Co(10–10) Surface: The Effect of Crystal Facets on the Preferred Mechanism. *Comput. Mater. Sci.* **2018**, *145*, 263–279.

(57) Yao, M. Q.; Wang, B. J.; Sun, B. L.; Luo, L. F.; Chen, Y. J.; Wang, J. W.; Wang, N.; Komarneni, S.; Niu, X. B.; Hu, W. C. Rational Design of Self-supported Cu@WC Core-shell Mesoporous Nanowires for pH-universal Hydrogen Evolution Reaction. *Appl. Catal. B: Environ.* **2021**, *280*, 119451.

(58) Kelly, T. G.; Ren, H.; Chen, J. G. Decomposition Pathways of C_2 Oxygenates on Rh-modified Tungsten Carbide Surfaces. *Surf. Sci.* **2015**, *640*, 89–95.

(59) Wang, B. J.; Liang, D. L.; Zhang, R. G.; Ling, L. X. Crystal Facet Dependence for the Selectivity of C_2 Species over Co_2C Catalysts in the Fischer–Tropsch Synthesis. *J. Phys. Chem. C* **2018**, *122*, 29249–29258.

(60) Zhang, R. G.; Wen, G. X.; Adidharma, H.; Russell, A. G.; Wang, B. J.; Radosz, M.; Fan, M. H. C_2 Oxygenate Synthesis via Fischer–Tropsch Synthesis on Co_2C and Co/Co_2C Interface Catalysts: How to Control the Catalyst Crystal Facet for Optimal Selectivity. *ACS Catal.* **2017**, *7*, 8285–8295.

(61) Griboval-Constant, A.; Giraudon, J. M.; Twagishema, I.; Leclercq, G.; Rivas, M. E.; Alvarez, J.; Perez-Zurita, M. J.; Goldwasser, M. R. Characterization of New Co and Ru on α -WC Catalysts for Fischer–Tropsch Reaction: Influence of the Carbide Surface State. *J. Mol. Catal. A: Chem.* **2006**, *259*, 187–196.

(62) Christensen, J. M.; Duchstein, L. D. L.; Wagner, J. B.; Jensen, P. A.; Temel, B.; Jensen, A. D. Catalytic Conversion of Syngas into Higher Alcohols over Carbide Catalysts. *Ind. Eng. Chem. Res.* **2012**, *51*, 4161–4172.

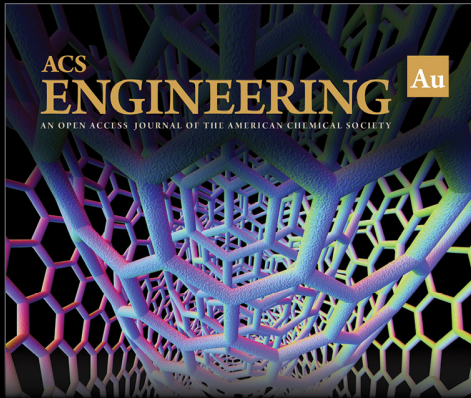
(63) Dongil, A. B.; Zhang, Q.; Pastor-Pérez, L.; Ramírez-Reina, T.; Guerrero-Ruiz, A.; Rodríguez-Ramos, I. Effect of Cu and Cs in the β - Mo_2C System for CO_2 Hydrogenation to Methanol. *Catalysts* **2020**, *10*, 1213.

(64) Xiang, M. L.; Li, D. B.; Li, W. H.; Zhong, B.; Sun, Y. H. Potassium and Nickel Doped β - Mo_2C Catalysts for Mixed Alcohols Synthesis via Syngas. *Catal. Commun.* **2007**, *8*, 513–518.

(65) Zhang, L. F.; Ball, M. R.; Liu, Y. F.; Kuech, T. F.; Huber, G. W.; Mavrikakis, M.; Hermans, L.; Dumesic, J. A. Synthesis Gas Conversion over Rh/Mo Catalysts Prepared by Atomic Layer Deposition. *ACS Catal.* **2019**, *9*, 1810–1819.

(66) Rodriguez, J. A.; Evans, J.; Feria, L.; Vidal, A. B.; Liu, P.; Nakamura, K.; Illas, F. CO_2 Hydrogenation on Au/TiC, Cu/TiC, and Ni/TiC Catalysts: Production of CO, Methanol, and Methane. *J. Catal.* **2013**, *307*, 162–169.


(67) Koverga, A. A.; Flórez, E.; Dorkis, L.; Rodriguez, J. A. Promoting Effect of Tungsten Carbide on the Catalytic Activity of Cu for CO_2 Reduction. *Phys. Chem. Chem. Phys.* **2020**, *22*, 13666–13679.




ACS
ENGINEERING Au
AN OPEN ACCESS JOURNAL OF THE AMERICAN CHEMICAL SOCIETY

Editor-in-Chief: **Prof. Shelley D. Minteer**, University of Utah, USA

Deputy Editor:
Prof. Vivek Ranade
University of Limerick, Ireland

Open for Submissions 

pubs.acs.org/engineeringau  ACS Publications
Most Trusted. Most Cited. Most Read.